BULLETIN OF THE EARTHQUAKE
RESEARCH INSTITUTE
UNIVERSITY OF TOKYO
Vol. 66 (1991), pp. 351-381

Aftershock Distribution of the 1990 Rudbar, Northwest Iran, Earthquake of M 7.3 and Its Tectonic Implications

Tameshige TSUKUDA[1], Kaname SAKAI[1], Shin'ichi HASHIMOTO[1], Mohammad Reza GHEITANCHI[1], Soleiman SOLTANIAN[2], Parviz MOZAFFARI[2], Naser MOZAFFARI[2], Bahram AKASHEH[2] and Abdolrahim JAVAHERIAN[2]

[1] Earthquake Research Institute, University of Tokyo
[2] Institute of Geophysics, Tehran University

(Recieved April 1, 1991)

Abstract

One of the largest earthquakes in Iran occurred on June 20, 1990, at 21:00 UT at around Rudbar and Manjil Cities in Gilan Province, northwest Iran. An aftershock observation has been conducted around the source region from 30 days after the mainshock and has been continued for more than 5 months. The epicenters of the aftershocks are extending as long as 90 km striking WNW–ESE in parallel with the trend of the northern and southern marginal longitudinal faults of the Qezel-Owzan basin along the Talesh-Alborz seismo-tectonic zone. A strike-slip fault, running along the aftershock zone on the uplifted side of the northern marginal fault, is proposed judging from the topographic map and the Landsat image.

The part of the aftershock area southeast of the main shock epicenter is more active than the northwestern part. Particularly, microseismic activity is very high in the southeastern end close to Pakdeh, where remarkable surface fissures were observed.

The V_P/V_S ratio is inferred as 1.88 ± 0.60 for the region covered by the seismic network. The aftershock decay rate was such that $p=1.5$ for the modified Omori formula, although the p value for a short period of 4 days at the beginning of the observation was around 4.0.

1. Introduction

On June 20, 1990, at 21 : 00 UT a shallow destructive earthquake attacked the region centering on the Township of Rudbar, Gilan Province, northwest Iran. A preliminary report issued five days after the earthquake by the Institute of Geophysics, Tehran University

(hereafter abbreviated as IGT) describes the hypocentral parameters for the mainshock as follows:

Origin Time: June 20, 21 : 00 : 13.12 UT;
Hypocenter: 36°49.00'N, 49°24.51'E, Depth=10 km;
Local Magnitude: 7.3.

This event was one of the largest in recent times in Iran, which is situated in the Alpine-Himalaya seismic belt. It caused severe damage to human lives and structures in the Gilan and Zanjan Provinces, particularly in the cities in the Sefidrud and Shah Rud river valleys, as well as villages in the mountainous areas around the source region. The toll of lives amounted to several tens of thousands. Extensive field reports on this event have been published by MOINFAR and NADERZADEH (1990), ASTANEH and ASHTIANY (1990) and TSUKUDA *et al.* (1991).

We conducted seismic observations as a collaborate research program between IGT and Earthquake Research Institute, University of Tokyo a month after the occurrence of the M 7.3 event for more than five months. The main purpose of this project was to monitor the aftershock activity at a constant sensitivity level by a semi-permanent seismic network fully covering the source area. For a microseismic study, exploratory temporary observations were also carried out. This paper is the first detailed report of these observations.

2. Observation Stations and Instruments

The observation started on July 20, 1990. We set up 6 stations: three for a long term or semi-permanent observation and three for the short term. The coordinates of the stations and specifications of instruments are given in Tables 1 and 2. Some photographs showing the station sites and instruments are given in TSUKUDA *et al.* (1991). The sensors were Mark Products L type seismometers. The distribution of the stations is shown in Fig. 1 together with the IGT stations.

We employed the geographical map from the World Aeronautical and Operational Navigation Charts with a reduced scale of 1 : 500,000 as well as a 1 : 250,000 scale Iranian map to read the coordinates of the stations. The location of station ABT was determined by a simple triangulation to confirm the summit where the station is set up. The altitude data were mainly based on measurements by a small aneroid barometer. The accuracy of station locations is better than 1-3 km in horizontal coordinates and 100 m in altitude.

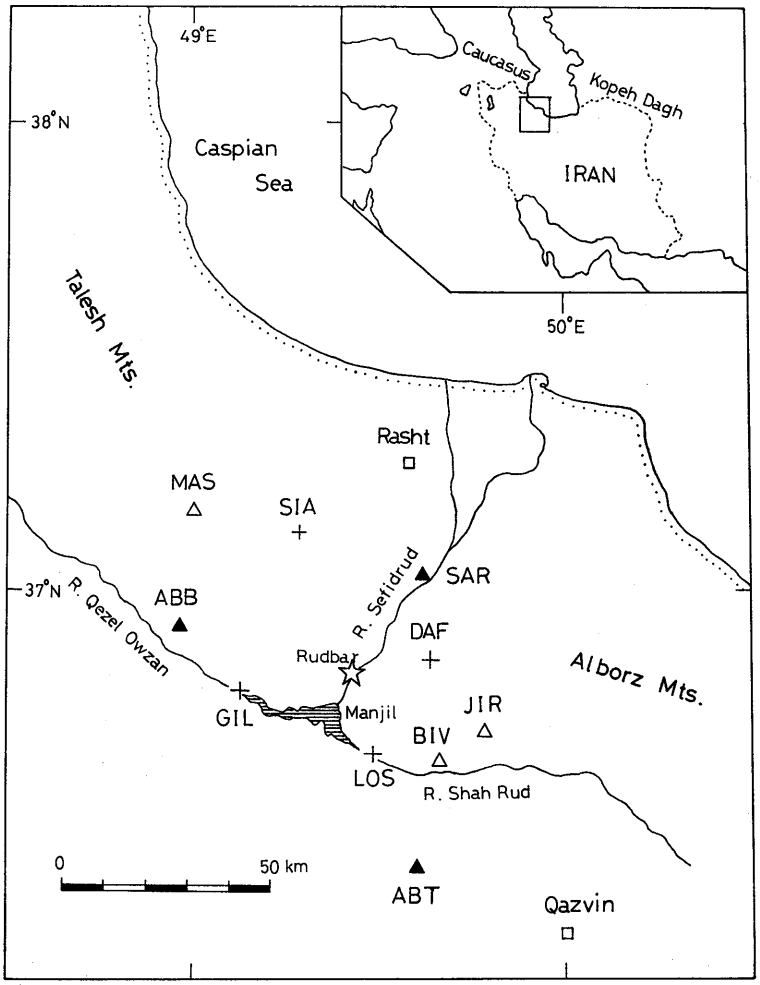

Fig. 1. Map showing the observation stations and the concerned regions. Solid triangles represent semi-permanent stations serving as a large tripartite network, whereas open rectangles indicate temporary stations. Stations marked by crosses belong to the Institute of Geophysics, Tehran University, and were operated with smoked paper drum recorders from several days after the mainshock until the end of September, 1990.

At the semi-permanent stations we installed the Takamisawa STR-100 seismo-recorders. This portable event recorder has won popularity in Japan for producing visible seismograms on a strip of paper with printed arrival times of seismic waves. The internal clock is specially designed to be calibrated by the radio timing signal broadcast hourly by NHK (Japan Broadcasting Corporation). Seismographs of this type were operated successfully in Turkey, and it was the first time in the

Table 1. Coordinates of the seismic stations and the observation periods. The origin of the x, y coordinates is (49.0° E, 37.0° N).

SITE	CODE	LONDITUDE (° E)	LATITUDE (° N)	ALTITUDE (m)	X(km) east	Y(km) north	PERIOD
Saravan	SAR	49.617	37.033	150	54.90	3.84	Jul.19-
Abbar	ABB	48.967	36.917	700	-2.94	-9.21	Jul.20-
Abtorsh	ABT	49.582	36.431	1900	52.19	-62.98	Jul.21-
Masuleh	MAS	48.992	37.167	800	-0.71	18.53	Jul.23-Jul.25
Bivarzin	BIV	49.667	36.633	900	59.65	-40.52	Jul.23-Jul.26
Jirandeh	JIR	49.783	36.697	1100	69.97	-33.34	Jul.22-Jul.26

Table 2. Specification of the instruments used. V and H mean vertical and horizontal components, respectively.

STATION	SENSOR TYPE		NATURAL FREQUENCY (Hz)	RECORDEER TYPE	SENSITIVITY 10^{-6}(cm/s)/mm	PAPER SPEED mm/s
SAR	L-4C	V	1.0	STR-100	467	4
ABB	L-22D	V	2.0	STR-100	560	4
ABT	L-22D	V	2.0	STR-100	1120	4
MAS	L-4C	V	1.0	MEQ-800	36.4	4
BIV	L-4C	V	1.0	MEQ-800	18.2	2,4
JIR	L-22D	V	2.0	DR-10		
	L-22H	H(2 sets)	2.0			

area outside Japan (TSUKUDA *et al.*, 1988). An example of the recorded waveforms is shown in Fig. 2.

Since an automatic calibration system for timing is not available in Iran as in Turkey, we had to calibrate the clock manually at a

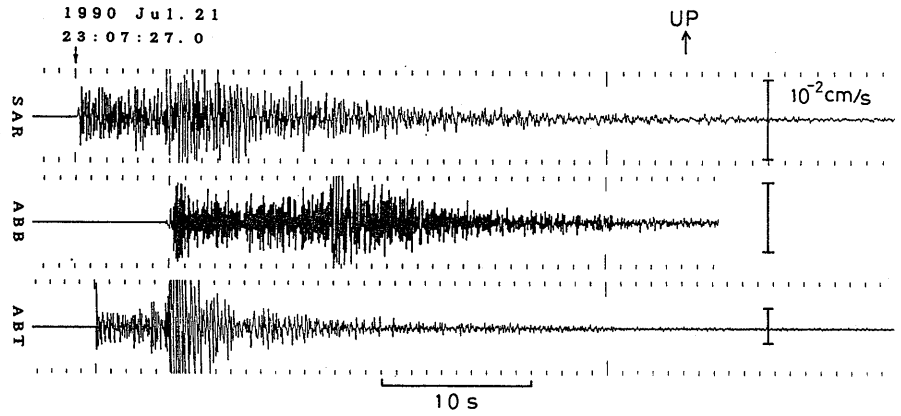

Fig. 2. Example of waveforms recorded at the semi-permanent stations.

certain time interval. We used Moscow radio on 15 MHz as a standard timing singnal. The measurement of the delay time (or advanced time) has been carried out making a time chart assuming a linear temporal variation of clock time. The delay rates were between -0.2 and -0.1 seconds a day.

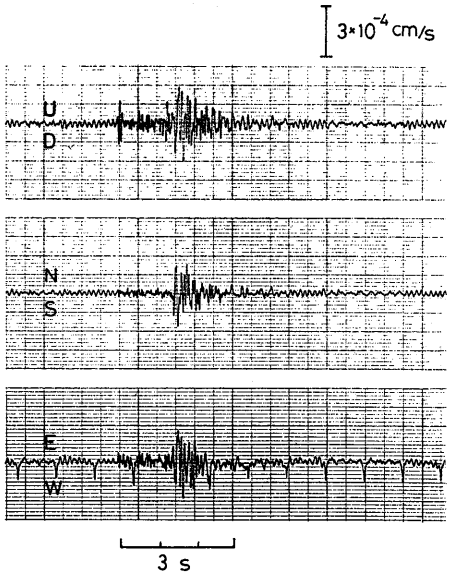

Fig. 3. Example of waveforms of a ultra-microearthquake recorded at Jirandeh Station (JIR).

The Saravan station (SAR) is located at the site of an institution for water supply controlled by the Ministry of Water and Power. We used a vacant small office building. The Abbar station (ABB) is set up on the basement floor in the oil storage house belonging to the town Board of Education. The Abtorsh station (ABT) is in the building of the national television relay station on top of a mountain. At the Bivarzin (BIV) and Masuleh (MAS) stations, we used the Sprengnether MEQ-800 ink writing helical drum recorders. The Jirandeh station (JIR) shared the place with that of IGT. Here we installed three component seismometers and a direct

recording cassette magnetic tape recorder (TEAC DR-10), providing us with a continuous record of the ground vibration during the period from July 22 to 26. The number of events identified on this record was more than 3000. One of the reproduced seismograms is shown in Fig. 3.

This paper deals with data from the 60 km-span tripartite network (SAR, ABB and ABT) during the period from July 20, to December 11, 1990 for SAR; from July 20, 1990 to January 4, 1991 for ABB; and from July 21, 1990 to January 4, 1991 for ABT, together with the data obtained from the temporary stations.

3. Aftershock Distribution Derived from the Large Tripartite Network

The number of shocks registered at all the three stations is 67 out of 790 earthquakes detected at at least one station. There are 54 events which have three P times and at least one S-P time data. In the following the procedures of hypocenter location and the data processing are summarized.

1) Reading of seismograms: The arrival times of P and S waves, polarities of initial motion, maximum amplitudes and final times of oscillation were digitized by a personal computer system developed by K. Sakai, one of the authors.

2) Time correction for each station: The measured delay times of the recorder clock are subtracted from the arrival times read on the seismograms.

3) Merging process of the observation data from different stations into combined observation data.

4) Determination of magnitudes. Since amplitude data were not always available due to clipping of waveforms, we adopted the following formula as a function of the total duration of oscillation.

$$M=\alpha\cdot\log(\text{F-P})+\beta \qquad (1)$$

F-P time (P time to Final time) is given in seconds. α is assumed to be 2.85 according to the study by TSUMURA (1967). To determine the value of β, we need some reference magnitude data. During the observation, three events (Events No. 19, 20, and 21 in Table 3) were reported by USCGS as QED (Quick Epicenter Determination). Based on the reported body-wave magnitudes we obtained $\beta=-1.33$ by the method of least squares.

5) Estimation of V_P/V_S ratios from the Wadati diagrams. This process is useful to examine the accuracy of the readings of S arrival

Table 3. List of the Rudbar earthquake and large aftershocks reported by USCGS (QED) during the period from June to December, 1990.

No.	ORIGIN TIME (UT)					LATITUDE (° N)	LONGITUDE (° E)	DEPTH (km)	MAGNITUDE		STANDARD DEVIATION (s)	NUMBER OF STATIONS
	M	D	H	M	S				Mb	Ms		
1	Jun.	20	21	00	09.0	37.047	49.384	10	6.4	7.6	1.2	147
2	Jun.	20	22	58	52.0	37.163	49.552	10	4.5		1.0	15
3	Jun.	20	23	00	39.0	37.45	49.55	10	5.1		0.7	6
4	Jun.	20	23	33	25.9	37.14	49.61	10	4.8		1.5	7
5	Jun.	21	00	22	33.7	37.36	49.51	10	4.6		0.7	6
6	Jun.	21	00	52	36.7	37.051	49.619	10	4.9		0.7	20
7	Jun.	21	02	08	51.7	36.927	49.812	10	5.4	4.6	0.9	118
8	Jun.	21	09	02	13.6	36.622	49.805	10	6.0	5.5	0.8	88
9	Jun.	21	12	17	27.3	36.762	49.391	10	4.8	3.9	1.2	22
10	Jun.	21	21	27	38.5	36.301	49.633	10	4.7		0.7	17
11	Jun.	24	09	45	56.8	36.825	49.452	10	5.1	4.5	1.0	79
12	Jun.	24	19	05	22.9	37.74	49.45	10	4.3		1.2	5
13	Jun.	26	19	03	16.0	37.63	49.89	10	4.1		1.4	7
14	Jun.	27	03	56	20.6	36.950	49.682	10	4.9		0.8	19
15	Jun.	28	03	20	36.0	37.122	49.606	10	4.8	4.1	1.1	23
16	Jun.	29	06	25	52.1	37.25	49.80	10	4.3		0.5	7
17	Jul.	1	17	19	44.4	37.385	48.965	10	4.5	3.5	1.4	22
18	Jul.	6	19	34	52.4	36.904	49.339	33	5.1	4.2	0.9	65
19	Aug.	13	06	18	26.7	36.937	49.854	33	4.8	3.6	1.1	14
20	Sep.	25	12	12	17.5	37.089	49.734	10	4.9		0.7	6
21	Oct.	17	17	06	29.2	36.974	49.385	33	4.5		0.4	8

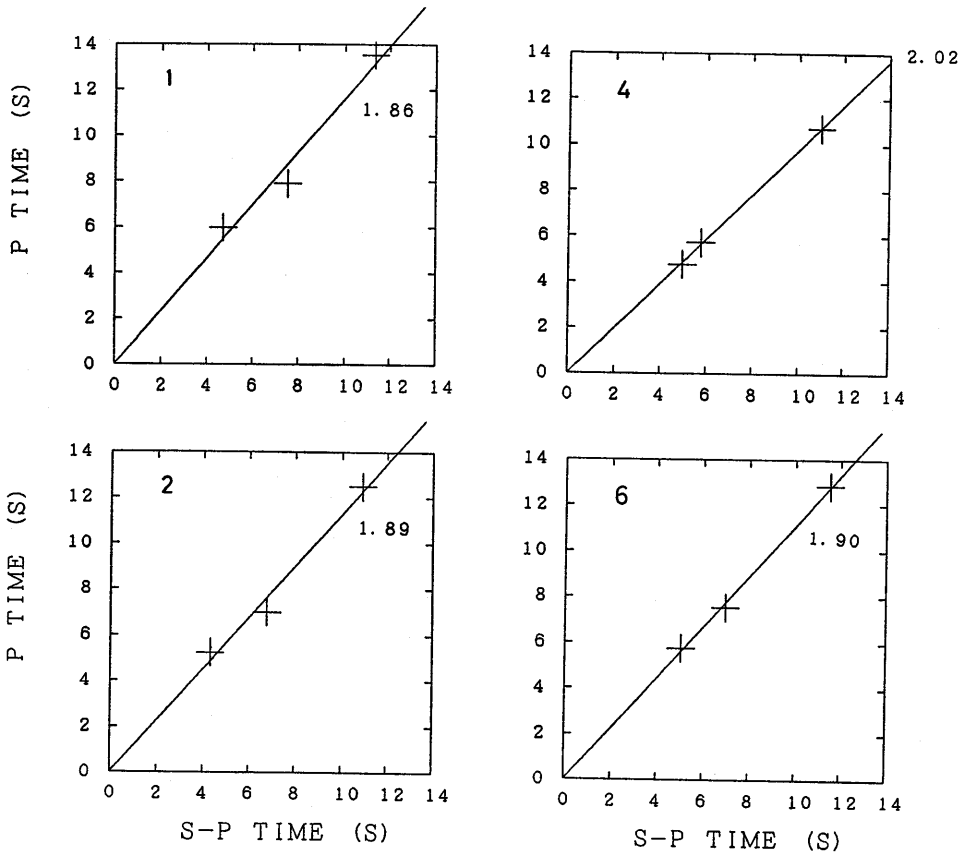

Fig. 4. Wadati diagrams (P time versus S-P time). Data from the three semi-permanent stations. The number on the left-hand side of each diagram is the event number in Table 4. The numeral on the right-hand side is the V_P/V_S ratio obtained by fitting the straight line as shown in the figure.

times. S waves are, in some cases, very difficult to interpret on seismograms. The V_P/V_S ratios were estimated for events recorded at the three semi-permanent stations. Figure 4 shows examples of fitting the regression line in the relation between P and S-P times. The average and the standard deviation of the V_P/V_S ratios for 19 events having three S-P time data are 1.88 and 0.6, respectively, where the data having S-P times over 14 s and such low quality data that the standard deviation of the residual of P times are beyond 1.0 s were excluded. BERBERIAN (1982) studied the aftershocks of the 1978 Tabas-e-Golshan earthquake in central Iran and obtained a similar V_P/V_S ratio of 1.85, which is much larger than that of the standard crust in Japan, where the ratios are around 1.7.

6) Computation of hypocenters. The method for three stations

is similar to that presented in the appendix of a previous paper (TSUKUDA *et al.*, 1977). The principle of its procedure is as follows:

The epicenter (x, y) should satisfy the following three equations:

$$(x-x_i)^2+(y-y_i)^2=r_i^2 \qquad (2)$$
$$i=1, 2, 3$$

where x_i, y_i and r_i are the coordinates and the epicentral distance for station i. We can calculate the epicentral distance if we know the focal depth h and the travel-time of P wave. The travel-time for a station is the arrival time (t_p) subtracted by the origin time t_0. The origin time is estimated as $t_0=t_p-(1/(V_P/V_S-1))(t_s-t_p)$ for each station, where t_s is S arrival time. Averaging the above origin times from different stations we obtain an optimum estimate of the origin time.

Equations (2) are reduced to the two linear equations by taking differences between two of Eqs. (2).

$$2(x_i-x_1)x+2(y_i-y_1)y=r_1^2-r_i^2+x_i^2-x_1^2+y_i^2-y_1^2 \qquad (3)$$
$$i=2, 3$$

The solution (x, y) is called radical center in geometry. This radical center is not always on the circles defined in (2). There are three cases of its position: (a) inside of the three circles; (b) on the three circles; (c) outside of the three circles. The function of origin time t_0 and focal depth h, $f(t_0, h)=1-r/R$, where r and R are the radius of the circle and horizontal distance of the radical center from a selected station, takes a negative, vanishing or positive value corresponding to (a), (b) and (c), respectively. In case (b), (x, y) is the solution for the epicenter, where a suitable focal depth h should be assigned.

We seek the solution changing the depth h. When no solution is found for a given range of h, we take (x, y) which gives the minimum of $|f(t_0, h)|$.

The computation of hypocenter requires a seismic velocity structure model. However, very little is known about the velocities in Iran, including our present field or the southern Caspian sea coast region along the Alborz mountains. AKASHEH (1975) studied travel-time residuals in the Iranian plateau with respect to a standard travel-time table to interprete the anomalies in terms of velocity variations in the crust or upper mantle under the stations in the respective regions. If the thickness of the crust is assumed to be uniform and as thick as 45 km in the whole area and no anomaly exists in the upper mantle, then the average crustal P velocity varies, ranging from 4.6 to 6.0 km/s from place to place. On the other hand, comprehensive investigations

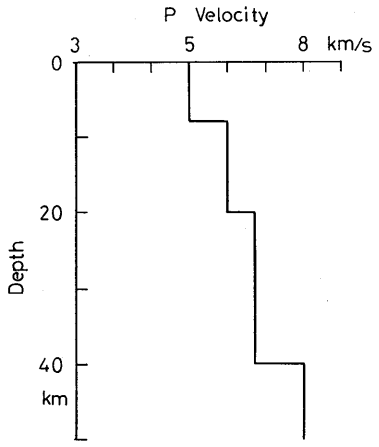

Fig. 5. P velocity structure model used for hypocenter determination.

of the crustal structure have been made by the methods of seismic sounding and drilling in the southern part of the Caspian Sea region, adjacent to our sites (NEPROCHNOV, 1968; SHIKALIBEILY and GRIGORIANTS, 1980). The thickness of the crust in this region is very variable, from 35 km to 47 km. The structure is characterized by very thick sedimentary layers and absence of the so-called granitic layer in some parts.

Taking account of the above knowledge, we made up a simple P velocity model as shown in Fig. 5. As confirmed by the explosion seismic experiment (IKAMI *et al.*, 1988), near surface sediments have a high value of V_P/V_S, as much as 2.0. Therefore, the relatively thick sedimentary layer represented by a P velocity of 5 km/s is consistent with high values of V_P/V_S ratio. The S velocity in our model is deduced from the inferred V_P/V_S ratio of 1.88. The thick sedimentary layer is also preferable to account for an interrelation between focal depths and an S-P time distribution as will be discussed in Section 5. Otherwise, if the discontinuity between the top and the second layers is raised, the focal depths increase to some extent at the southeastern end of the aftershock zone. The topographic time correction for each station, which should be subtracted from the arrival time data, was defined to be the altitude divided by the top layer velocity.

The located local earthquakes are listed in Table 4. The epicentral distribution is given in Fig. 6. Three dimensional plots of hypocenters are shown in Figs. 7 and 8. They exhibit a 90 km long linear alignment of epicenters in an N 60°W direction, suggesting that the mainshock generated a nearly vertical fault.

In order to estimate the accuracy of the hypocenters, we performed a simulation of hypocenter location (Fig. 9). The assigned errors in P and S-P times are ± 0.3 s, which is the probable maximum error. The extent of the distributed hypocenters for each reference event represents the maximum hypocentral errors. As seen from the figure, the epicenter is well constrained within 4 km in radius, whereas the

Table 4. List of hypocenters determined by the use of data from SAR, ABB and ABT stations. The parameters for the main shock reported by Institute of Geophysics, Tehran University are also given on the last line. V_P/V_S values are listed if the event has three S-P time data and the standard deviation (S.D.) of P residuals is less than 1.0 s.

No.	ORIGIN TIME (UT)		LAT	LON	DEPTH	X	Y	M	Vp/Vs	S.D.
	Y M D H M	S	(° N)	(° E)	(km)	(km)				
1	90 7211817	54.1	36.631	49.811	17.9	72.6	-40.6	3.2	1.86	0.60
2	90 7211845	11.4	36.645	49.742	15.6	66.3	-39.1	3.1	1.89	0.44
3	90 7212249	48.5	36.634	49.810	19.3	72.4	-40.3	3.6		
4	90 72123 7	19.3	36.667	49.722	21.8	64.5	-36.8	4.0	2.02	0.08
5	90 7212344	5.9	36.519	49.830	28.0	74.3	-53.0	3.7		
6	90 722 0 9	23.0	36.631	49.802	22.3	71.7	-40.6	3.1	1.90	0.14
7	90 722 1 4	34.1	37.318	52.731	87.4	330.8	41.8	4.2		
8	90 722 449	39.4	36.753	49.512	4.9	45.7	-27.3	4.3	2.00	0.48
9	90 7231533	39.1	36.735	49.640	65.8	57.2	-29.2	3.8		
10	90 7231730	33.0	36.858	49.357	26.8	31.8	-15.7	4.1		
11	90 7232134	5.6	36.737	49.593	6.4	53.0	-29.0	3.6	1.89	0.64
12	90 724 123	43.0	36.640	49.791	20.0	70.8	-39.7	4.2	1.95	0.19
13	90 724 3 7	43.4	36.721	49.356	57.4	31.8	-30.9	3.0	2.11	0.23
14	90 724 727	16.6	36.651	49.769	26.1	68.7	-38.5	4.8		
15	90 724 831	12.7	36.721	49.356	30.8	31.8	-30.9	3.5		
16	90 8 71658	23.6	36.721	49.356	60.4	31.8	-30.9	3.3	1.83	0.24
17	90 8111638	5.9	37.661	49.048	-3.0	4.2	73.4	4.2		
18	90 8121710	28.3	36.726	49.640	31.0	57.1	-30.2	3.9		
19	90 813 4 6	50.5	36.689	49.795	24.5	71.0	-34.2	3.9	0.90	0.21
20	90 81623 3	34.5	36.621	50.746	89.0	156.2	-40.6	3.6		
21	90 8191915	35.0	36.278	51.148	35.6	193.0	-78.0	3.8		
22	90 8211252	40.3	36.710	49.468	7.6	41.9	-32.0	3.6	2.56	0.32
23	90 824 911	58.5	37.004	49.258	22.1	23.0	0.5	3.5		

Table 4. (Continued)

No.	ORIGIN TIME (UT) Y M D H M	S	LAT (° N)	LON (° E)	DEPTH (km)	X (km)	Y (km)	M	Vp/Vs	S.D.
24	90 8271736	57.4	36.656	49.605	25.0	54.1	-38.0	3.7	1.81	0.03
25	90 8271938	2.0	37.029	49.143	65.0	12.7	3.3	3.4		
26	90 8282234	10.3	37.042	49.104	36.1	9.3	4.6	4.0		
27	90 829 123	26.3	35.078	49.422	16.6	38.5	-213.2	3.8		
28	90 829 5 3	5.6	36.721	49.356	58.0	31.8	-30.9	3.5		
29	90 829 837	55.6	36.907	49.348	27.5	31.0	-10.3	3.6	2.84	0.52
30	90 917 7 3	40.0	36.858	49.357	14.4	31.8	-15.7	4.3		
31	90 917 739	36.6	36.213	50.241	85.6	111.6	-86.6	4.3		
32	90 9202121	13.6	36.885	49.180	19.1	16.0	-12.8	3.5	1.46	0.86
33	9010 2 141	57.7	36.722	49.356	43.9	31.8	-30.8	3.9		
34	9010 3 455	32.1	36.757	49.530	26.5	47.3	-26.8	3.4	2.72	0.37
35	9010122030	16.1	36.337	50.320	12.8	118.5	-72.8	4.1		
36	901129 8 9	9.0	36.423	51.208	30.9	198.1	-61.8	3.7		
37	9012 31420	28.3	36.689	49.741	78.5	66.2	-34.3	3.3		
38	9012 320 6	26.8	36.722	49.356	65.0	31.8	-30.8	4.0		
39	901211 921	30.5	36.721	49.356	83.8	31.8	-30.9	3.8		
	90 6202100	13.1	36.817	49.409	10.0	36.5	-20.2	7.3		
			(Main-Shock)							

focal depth solution is quite unstable, splitting into two groups: near surface and around the reference focus. In addition to the above hypocentral errors, there are errors due to the uncertainty of station coordinates. The epicentral errors are roughly comparable to those of the coordinates of the stations.

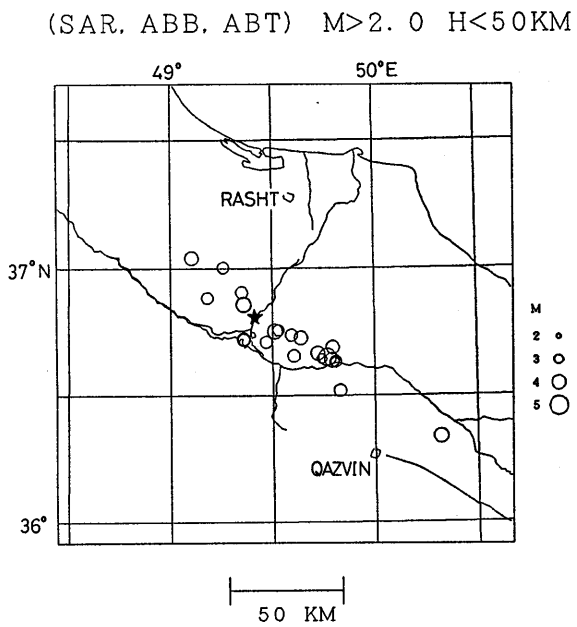

Fig. 6. Epicentral distribution of aftershocks using data from the semi-permanent stations. The star is the epicenter of the mainshock.

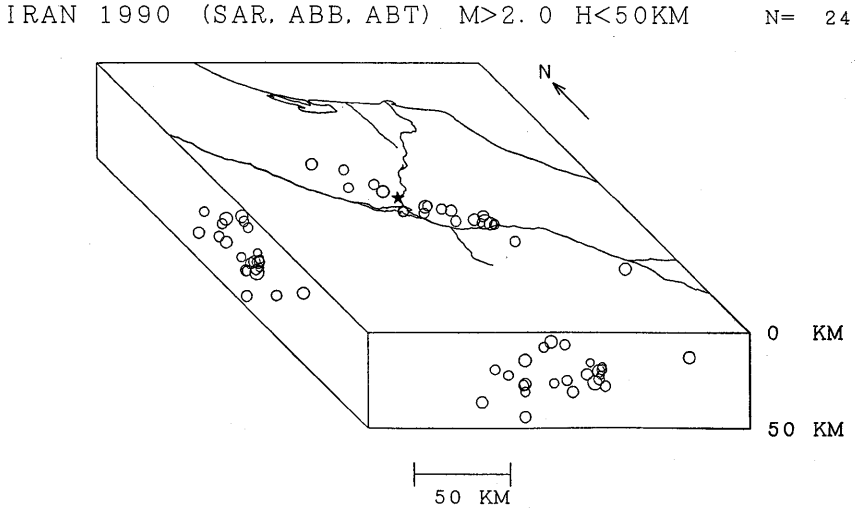

Fig. 7. Three dimensional distribution of aftershocks using data from the semi-permanent stations.

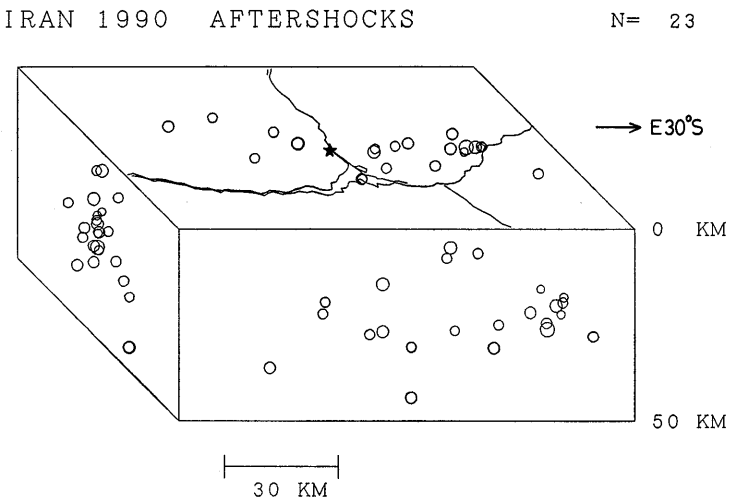

Fig. 8. Close-up aftershock distribution, similar to that in Fig. 7.

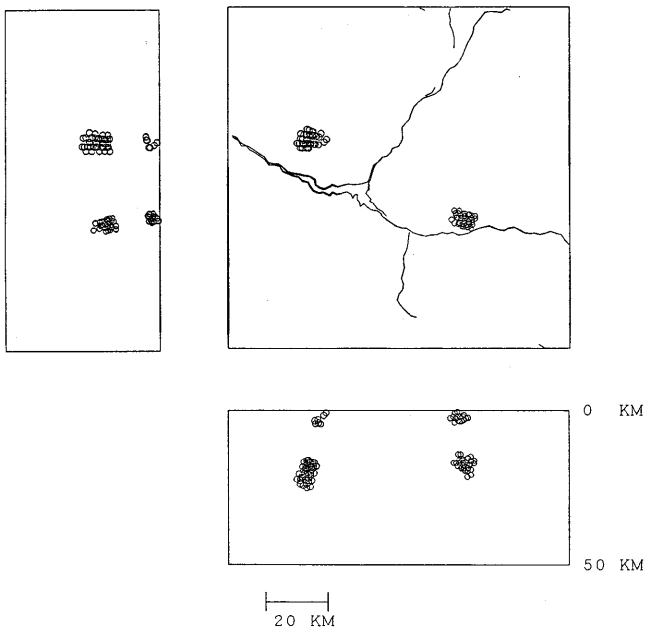

Fig. 9. Simulation of hypocentral errors. The two events (Nos. 2 and 32 in Table 4) are taken as examples. Assigned arrival time errors are ± 0.3 s in both P and S–P times. These values were added to the arrival time data at the stations chosen by a random sampling method. The simulated foci are plotted on the epicentral map and vertical cross sections.

4. Aftershock Distribution Derived from Four Stations or More

This section describes the result of hypocenter determination using both short-term and long-term observation data. The V_P/V_S ratios from the stations close to the source area are lower than the results mentioned in the last section; some events take values as low as 1.64–1.72 (Fig. 10); the average is 1.74 ± 0.09 for 13 events during four days from July 23 to 25. The reason for this is considered to be either that small values reflect local velocity structure, or there are differences in appearence of seismic waves between nearby and distant stations.

A kind of Baysian non-linear inversion technique developed by

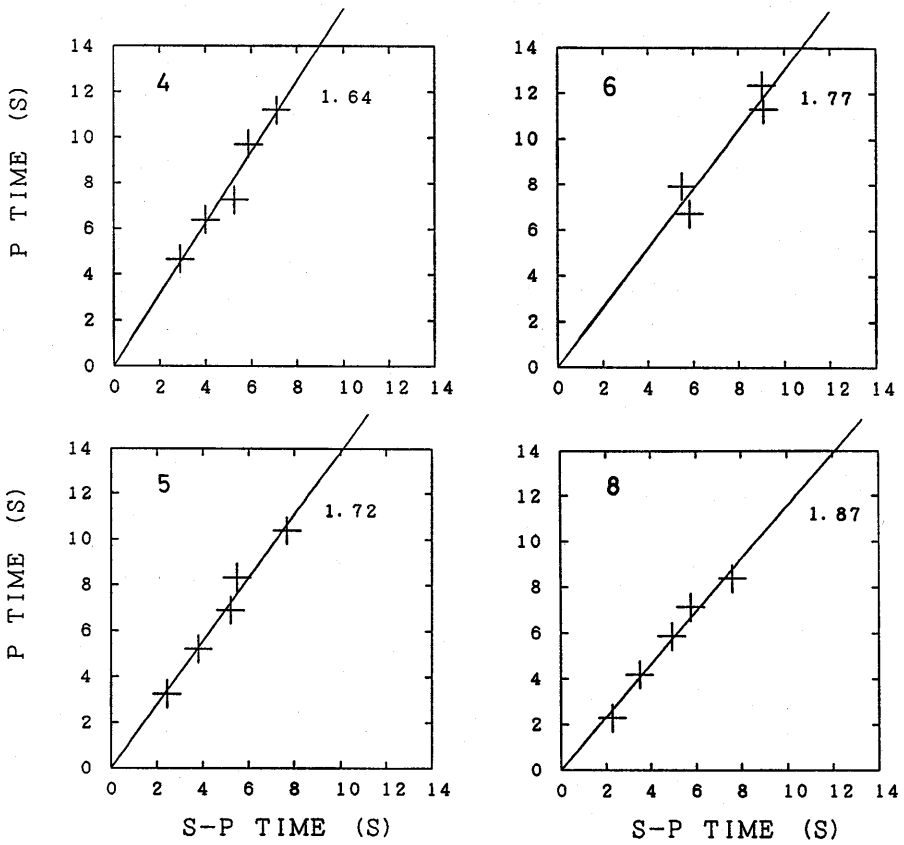

Fig. 10. Wadati diagrams for the events showing relatively low values of V_P/V_S. Data from temporary stations are also employed. The event numbers similar to Fig. 4 refer to those in Table 5.

Table 5. List of hypocenters determined by the use of four stations or more. N means the number of stations used in the hypocenter determination in Section 4. V_P/V_S values are given with the number of S–P data (n).

No.	ORIGIN TIME (UT) Y M D H M S	LAT (° N)	LON (° E)	DEPTH (km)	N	MEAN O-C P (s)	MEAN O-C S (s)	X (km)	Y (km)	M	Vp/Vs	S.D.	n
1	90 7231049 22.0	36.915	49.192	-0.0	4	0.91	0.25	17.1	-9.4	4.0	1.73	0.01	3
2	90 7231533 43.3	36.776	49.495	5.0	5	0.73	0.31	44.2	-24.8	3.8			
3	90 7231730 25.6	36.887	49.171	28.3	6	0.81	0.62	15.3	-12.6	4.1	1.60	0.25	3
4	90 7231819 23.0	36.772	49.458	0.8	5	0.79	1.31	40.9	-25.2	2.6	1.64	0.50	5
5	90 7231941 0.3	36.751	49.473	-0.6	5	0.92	1.34	42.2	-27.5	2.7	1.72	0.37	5
6	90 7232134 4.5	36.751	49.562	-9.0	6	0.62	1.17	50.2	-27.5	3.6	1.77	0.71	4
7	90 724 123 42.5	36.662	49.887	16.0	6	0.51	0.51	79.3	-37.1	4.2	1.85	0.56	4
8	90 724 3 7 42.6	36.748	49.515	-3.4	5	0.62	0.83	46.0	-27.8	3.0	1.87	0.33	5
9	90 724 727 16.7	36.708	49.712	-6.0	4	0.30	0.40	63.6	-32.1	4.8			
10	90 724 831 7.1	36.768	49.544	-7.8	4	0.53	0.06	48.6	-25.6	3.5			
11	90 7241127 5.0	36.782	49.390	-1.0	4	0.61	0.33	34.8	-24.1	4.0	1.75	0.42	3
12	90 7241555 5.9	36.795	49.584	3.1	4	0.09	0.43	52.1	-22.6	3.0	1.71	0.40	3
13	90 7241555 59.7	36.712	49.778	11.4	4	0.32	0.20	69.5	-31.6	2.6			
14	90 7241727 36.7	37.063	49.028	-6.6	4	0.62	0.33	2.5	7.0	3.5			
15	90 72418 3 37.7	36.941	49.196	-0.3	4	0.38	0.22	17.4	-6.5	3.1	1.62	0.83	3
16	90 7242127 46.5	36.602	49.921	-0.4	4	0.48	0.44	82.4	-43.8	3.2	1.88	0.29	3
17	90 7242323 25.5	37.047	48.922	-1.2	4	0.62	0.34	-6.9	5.3	2.8	1.78	0.29	3
18	90 7251647 29.1	36.769	49.754	-3.7	4	0.44	0.98	67.3	-25.4	2.6	1.71	0.72	4
19	90 7251656 2.3	36.867	49.269	-20.3	4	0.39	0.09	24.0	-14.7	3.8			
20	90 7251842 17.9	36.884	49.047	-17.8	4	0.35	0.08	4.1	-12.9	3.7			

MATSU'URA (1984) and HIRATA and MATSU'URA (1987) was used for computing hypocenters with a priori arrival time errors of 0.3 s for both P and S waves. The assigned V_P/V_S value is 1.80 for this case. Other conditions are the same as in Section 3. The hypocentral data are given in Table 5 and Fig. 11.

The differences between observed and calculated travel-times (O–C) are rather large, some events showing more than 1 s for S waves and

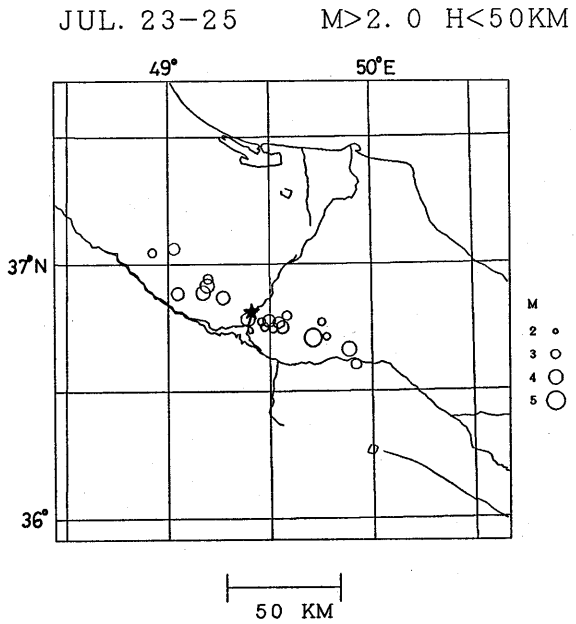

Fig. 11. Epicentral distribution of the aftershocks determined by four stations or more. Star indicates the epicenter of the mainshock.

great discrepancies in epicenters more than 10 km (Tables 4 and 5). This may be attributed partly to the uncertainty of the positions of the stations and the timing of the recorders. However, the authors believe the main reason to be the complexity of the upper crustal structure. This is quite probable: For instance, in the Shin'etsu region, in central Honshu, Japan, which has many active faults and folds similar to the concerned region in Iran, there are anomalous travel-time residuals reaching 1.0 s at relatively short distances of 40 km (University of Tokyo, 1987).

5. Other Properties of Aftershock Activity

5.1. S-P Time Distribution

Microearthquake activity was properly monitored at the temporary stations. The S-P time distributions are given in Figs. 12, 13 and 14. At JIR a predominant frequency peak occurs at around 1-2 s. The hypocentral distances of these clustered earthquakes range from 6 to 16 km, provided that the Omori coefficient for our region is in range between 6.0 to 8.0. Such events should correspond to the clustering foci at depths ranging from 16 to 28 km at the southeastern end of the aftershock zone (Figs. 6~8; Table 4). However, the expected

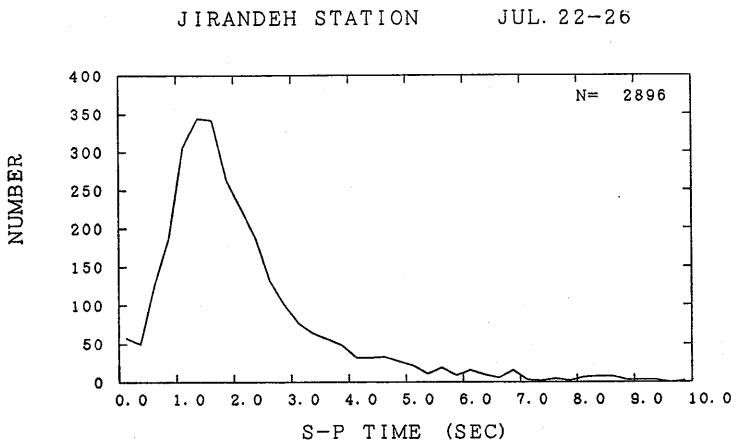

Fig. 12. S-P time distribution at Jirandeh Station (JIR).

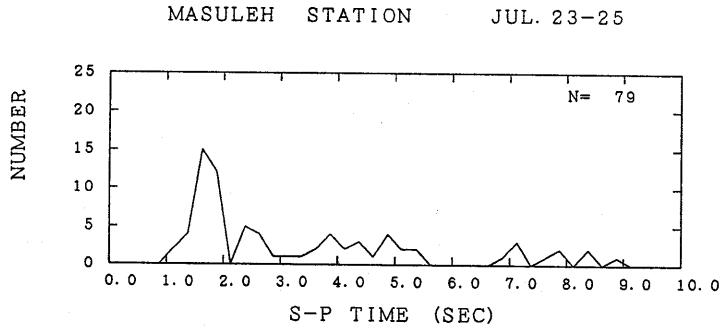

Fig. 13. S-P time distribution at Masuleh Station (MAS).

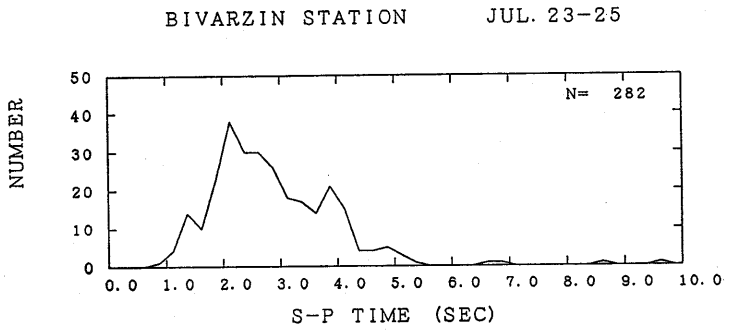

Fig. 14. S-P time distribution at Bivarzin Station (BIV).

depths from the S-P time distribution are not more than 16 km. This implies that the calculated hypocenters are to be corrected by reducing at least several kilometers in focal depth. It is probable that the

true epicenters are a little closer to the Jirandeh station. Consequently, the swarm-like aftershocks in the vicinity of Jirandeh and Pakdeh took place 5–10 km south of station JIR at a depth shallower than 16 km. The focal region is also within 5 km southeast of Pakdeh, 4 km southwest of Jirandeh.

The predominant S-P times are between 2.0 s and 3.0 s at Bivarzin (Fig. 14). Their corresponding events may also cluster in the vicinity of Pakdeh. There is a definite seismicity around the northwestern end of the aftershock zone as found in the S-P time distribution at Masuleh (Fig. 13).

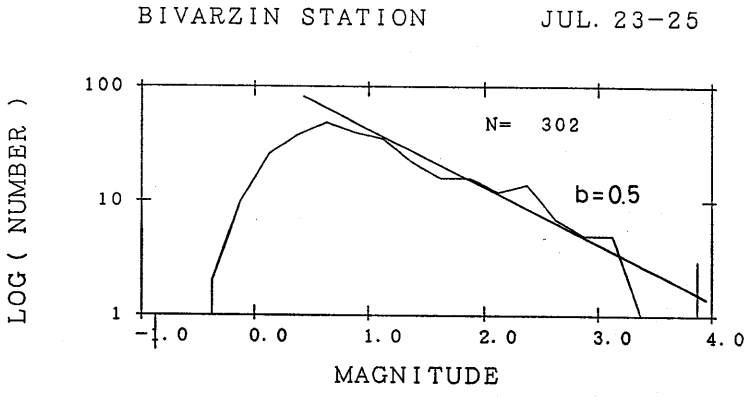

Fig. 15. Magnitude distribution at Bivarzin Station (BIV).

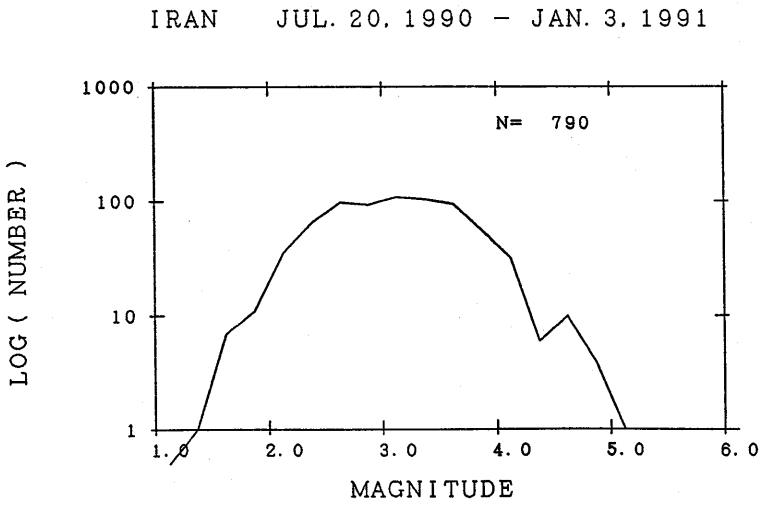

Fig. 16. Magnitude distribution for the semi-permanent network.

5.2. Magnitude Distribution

Figure 15 shows the magnitude distribution at Bivarzin. The F-P magnitude is also defined by formula (1) using $\beta=-2.36$ following experience in the Shin'etsu region, Japan. The linearity in the logarithmic graph holds for as small as 1 in magnitude; the Gutenberg-Richter's b value is 0.5.

The magnitude distribution of the earthquakes registered by the large tripartite network is shown in Fig. 16. Judging from the lack of smaller shocks, events with magnitudes above 3.0 would be detectable constantly in time by this network.

5.3. Temporal Change of the Activity

Figure 17 is the magnitude-time diagram. Shortage of recording paper forced suspension of the observation, particularly from the end of July to August 6, 1990. Occurrence frequency change of the earthquakes is given in Figs. 18 and 19. We observe the decrease of the activity with time. The decay rate or p value in the modified Omori formula is found to be 1.5 for the general trend during the period

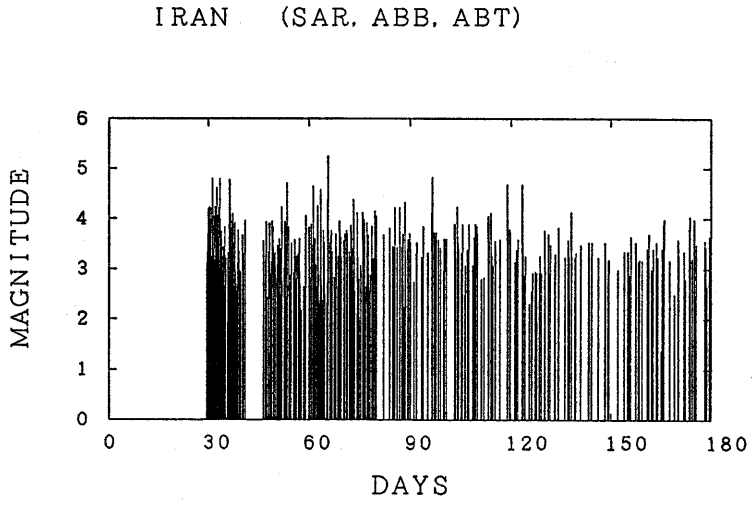

Fig. 17. Magnitude versus elapsed time for the events registered by the semi-permanent stations. Time is measured from the origin time of the main-shock. Relatively long suspension of observation is seen around the beginning of August. This is due to finishing of the recording paper. Such periods are as follows.

SAR: from 19:06, July 25 to 06:21, August 6;
ABB: from 14:56, July 28 to 11:13, August 6;
from October 22 to October 27;
from October 29 to November 15;
ABT: from 17:35, July 31 to 08:48, August 6.

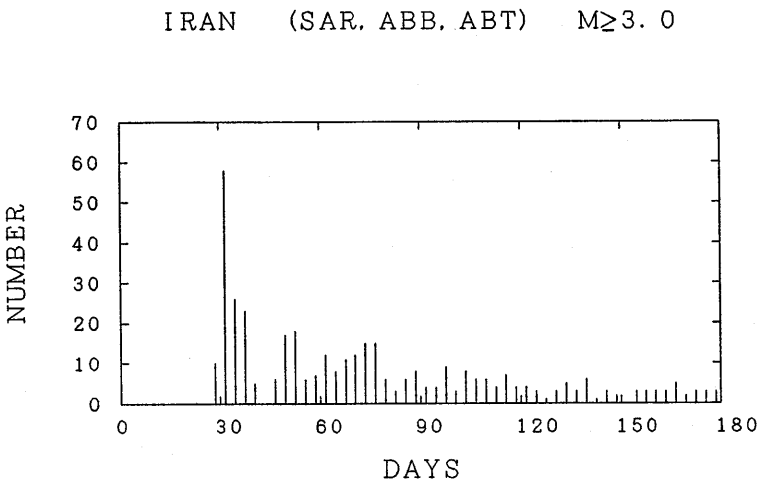

Fig. 18. Number of earthquakes with magnitude 3.0 or more for each three days registered at at least one station of the tripartite network.

from 30 days to 120 days after the mainshock. However, the numbers of events of the first several days are abnormally large compared with the subsequent periods, and the decay rate is much higher than the total trend. The microearthquake level also shows a high rate of decay ($p=4.0$) (Fig. 20).

UTSU (1969) studied and summarized the various properties of aftershocks for many events in and around Japan as well as around the world. In most cases, the p value is between 1.0 and 1.8. The majority (81.5%) of these have values less than 1.5. The 1956 Amorgos, Greece, earthquake of M 7.5 has the highest p value of 2.5.

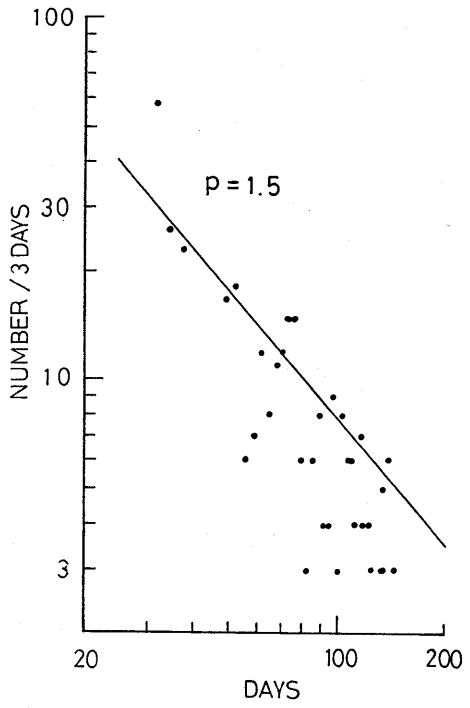

Fig. 19. Log-log plot of the frequency of the aftershocks as a function of time, similar to that in Fig. 18, excluding the data from periods when records were insufficient.

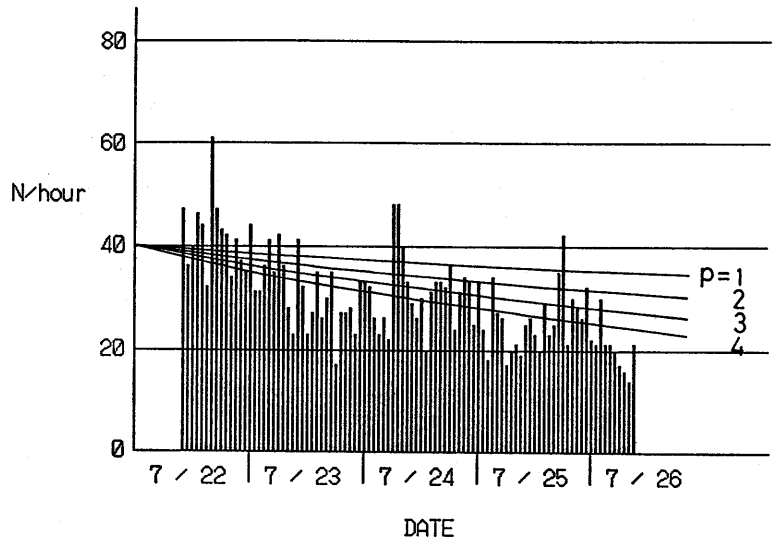

Fig. 20. Hourly number of shocks detected at Jirandeh Station. The solid curves represent the theoretical decay parameterized by p in the function $n(t) \propto t^{-p}$, where t is the elapsed time from the mainshock.

His paper treated no event in Iran. AMBRASEYS (1963) and KENNETH *et al.* (1969) presented time histograms of aftershocks in their papers for the 1962 Buyin-Zahra earthquake of M 7.3 and the 1968 Dasht-e-Bayaz earthquake of M 7.3, respectively. In both cases, the p values

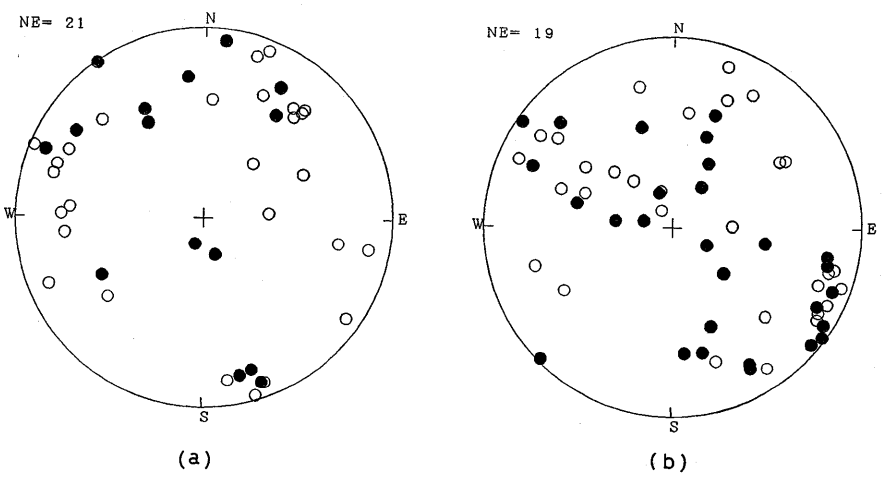

Fig. 21. Composite push-pull distributions of initial motion (equal area projection on the lower hemisphere). Solid and open circles represent compression and dilatation, respectively. Left: based on hypocentral data from three semi-permanent stations. Right: based on data from four stations or more.

are around 1.0 rather than 1.5.

Our data lacks events during the first month. The data from IGT will give the complete tendency of aftershock activity.

5.4. Focal Mechanisms

Because the number of our seismic stations is limited, focal mechanism solutions for respective events cannot be drawn. Figure 21 is the composite diagram for the focal mechanism. The angles of emergence were computed by use of the velocity model given in Fig. 5. Although no systematic fault plane solution is obtained, the compressional axis would strike in the E-W or SW-NE direction, similar to the mechanism of the mainshock given in Fig. 22. The irregular patterns of push-pull data in Fig. 21 imply that the focal mechanisms of aftershocks differ from event to event, suggesting complex rupture processes of aftershocks.

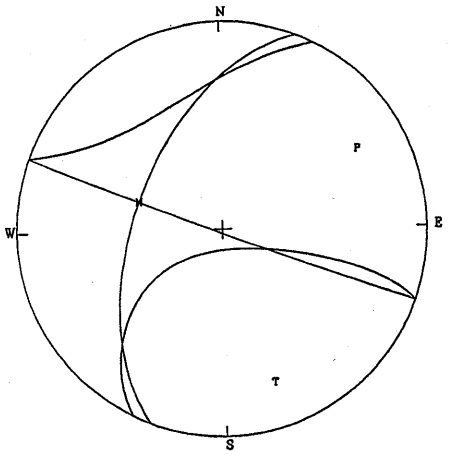

Fig. 22. Centroid-moment tensor solution and fault plane solution for the mainshock, after YOSHIDA (1990). P and T represent the pressure and tension axes.

6. Tectonic Implications and Discussion

The aftershocks took place along a narrow zone extending in the direction of about N50-60°W centered at the mainshock epicenter. Most of the foci are concentrated in the southeastern part of the aftershock zone. But a definite seismicity is observed in the northwestern part, the uplifted region north of Qezel-Owzan basin.

Figure 23 shows the topographic map around the source region of the Rudbar earthquake. The Qezel-Owzan basin, west of the Sefidrud reservoir and adjacent to the northwestern part of the aftershock zone, is a great graben, 80～100 km long and 15 km wide, surrounded by high mountains on both the northern and southern sides. At both margins of the basin at the 1000 m level, we recognize linearly trending steep scarps, of which cross sections are given in Fig. 24. These lineaments striking N62°W correspond to the dark strips on the Landsat image shown in Fig. 25. We interpret these paired lineaments **b** and **c** in Fig. 23 as longitudinal Quaternary active faults. At

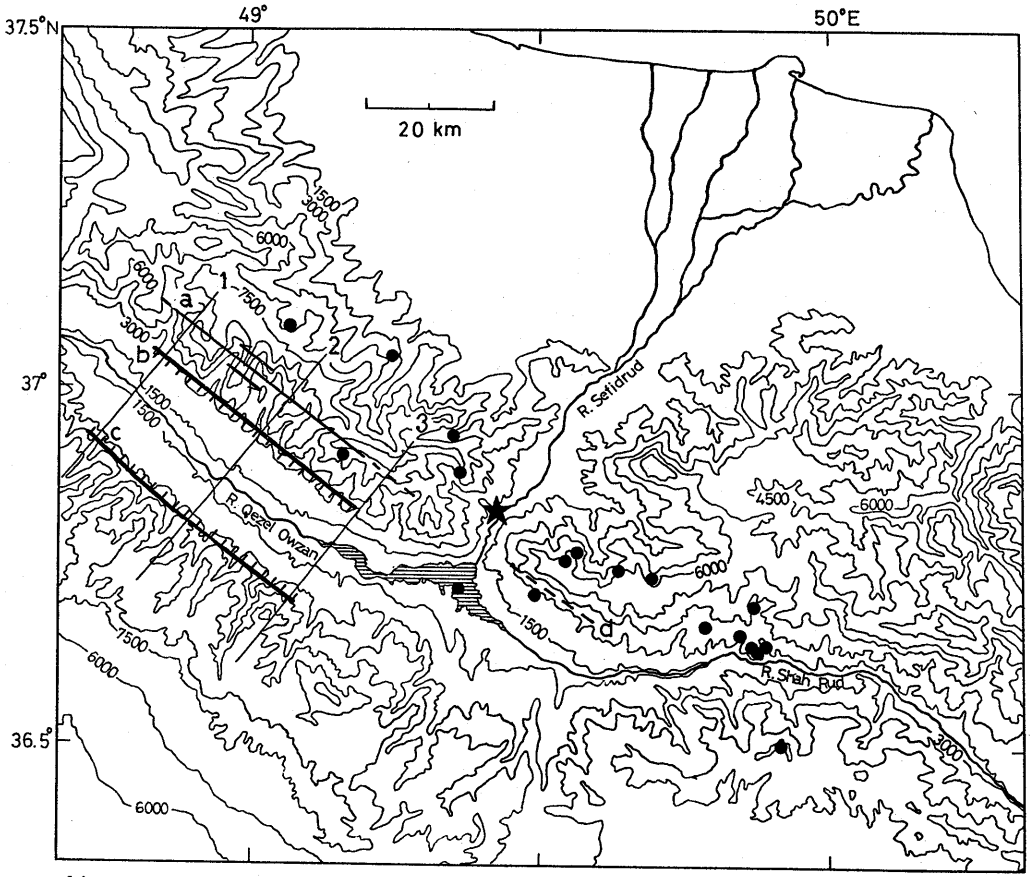

Fig. 23. Topographic map around the aftershock area. The contours are given in feet with an interval of 1500 feet. 1500, 3000, 4500, 6000, and 7500 feet are converted into 457, 914, 1372, 1829, and 2286 meters, respectively. The star indicates the epicenter of the mainshock. Solid circles are the aftershock epicenters determined in Section 3. The lineaments found in the topography are labeled by a, b, c and d. The fluff in the longitudinal faults b and c indicate the downthrown side.

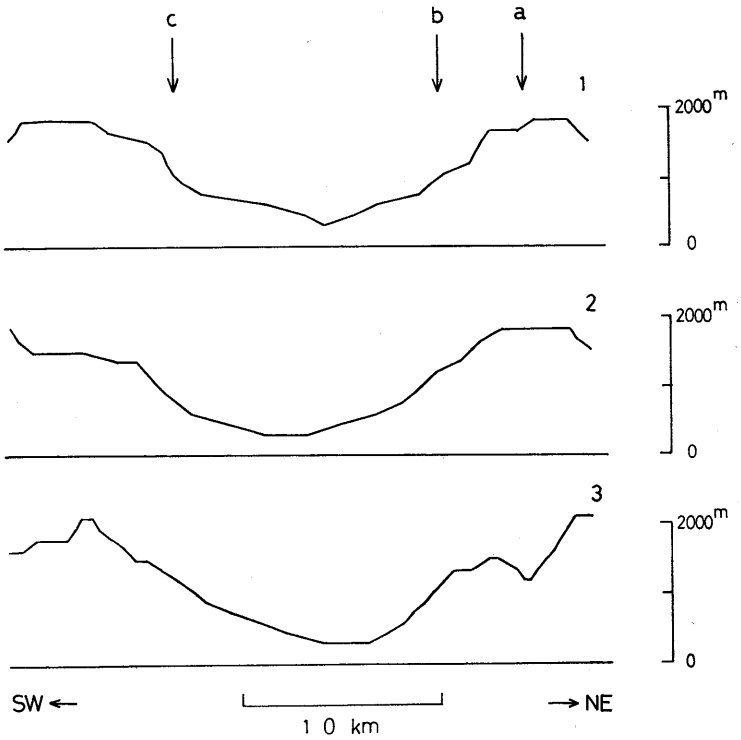

Fig. 24. Topographic cross section of the Qezel-Owzan basin. The profiles are shown in Fig. 23 with section Nos.

present, the authors have no data to confirm whether they are reverse or normal faults, or have any strike-slip components. The northern fault (**b**) may be a branch or part of the Masuleh fault whose trace is drawn in the seismo-tectonic map edited by BERBERIAN (1976). The longitudinal fault is interpreted to be a thrust fault (BERBERIAN, 1981).

The aftershocks have occurred on the northern uplifted side of the northern marginal fault, more than 5-6 km from the fault. Very close to this aftershock area, we can recognize another lineament (**a** in Fig. 23) in parallel with the above faults. The small ridges are offset more than 1-2 km left laterally. We propose that this lineament is evidence of a strike-slip active fault, which may explain well the inferred aftershock distribution and the focal mechanism of the M7.3 event.

On the other hand, around the aftershock zone on the eastern side of the Sefidrud river, no clear topographic lineament is found. There is only a 15 km long small-scale scarp several kilometers north of Manjil, trending WNW-ESE as an extention of the strike-slip fault. Moreover, we cannot find any evidence of lateral displacement for

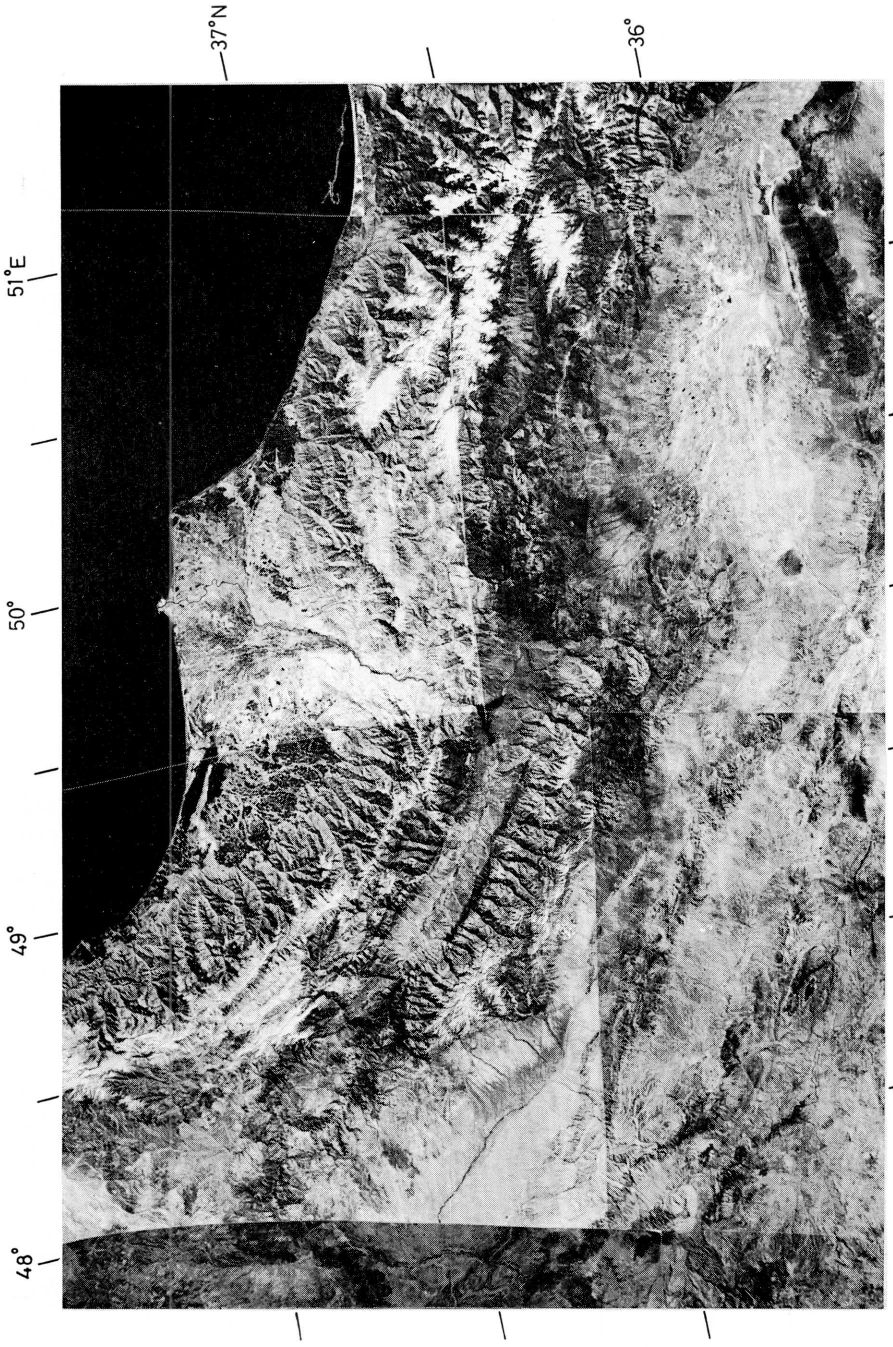

Fig. 25. Landsat mosaic imagery (ERT E-2078-06375-7, E-2078-06381-7, E-2078-06433-7, E-2078-06552-7 and others).

this. However, the authors believe that even such minor geomorphic features should not be ignored in the study of the seismo-tectonic properties.

It is presumable that the initial rupture of the Rudbar earthquake originated close to the southeastern end of the preexisting lateral fault. Reflecting the relaxation of stresses around the mainshock epicenter, there seems to be a 10–20 km wide seismicity gap in the aftershock zone. Here, it should be noted that even though the absolute positions of the gap for the two epicentral maps, Figs. 6 and 11, are different from each other, the relative distribution patterns are very similar. One can consider that this earthquake utilized the preexisting weak zone associated with the Quaternary fault to start the rupture. Then, the rupture might have propagated in both directions, northwest and southeast. According to KIKUCHI *et al.* (1990), the source process of this earthquake deduced from teleseismic waveforms suggests that southeastward propagated rupture was predominant. This is consistent with the high activity of aftershocks in the southeastern region. Probably, the rupture extended the fractured zone southeastwards into a region having a less fractured medium.

For understanding the generation of the fault system mentioned above, we need some knowledge of the geology and plate tectonics in and around Iran. The Iranian land mass is a continental block stressed by surrounding stable rigid plates, i.e., the Arabian plate, the Indian plate and the Eurasian plate. The strip zones that appear on the seismicity map are candidates for plate boundaries. Once LE PICHON (1968) regarded the Iranian region as a part of the Eurasian plate, whereas MORGAN (1968) assumed a plate boundary at around the Talesh-Alborz mountains separating Iran from Eurasia. On the other hand, MCKENZIE (1972) proposed the south Caspian micro-plate between the seismic zones, the Talesh-Alborz range and the Caucasus-Kopeh Dagh range. Moreover, NOWROOZI (1972) added some other micro-plates in and around the Iranian region.

The studies of focal mechanisms reveal that the Iranian plateau is being compressed in a north-to-northeast direction mainly by northern and southern blocks of greater rigidity, i.e., the Eurasian and Arabian plates, and undergoes shortening and thikening of the continental crust (MCKENZIE, 1972; NOWROOZI, 1972; JACKSON and MCKENZIE, 1984). Moreover, it is laterally trapped between the Arabian plate with eastern Asia-Minor in the west and the Indian plate with Eurasia in the east, which prevents the movement of any of the continental blocks forming the Iranian plateau sideways across lateral faults other than the movement of shortening by reverse faulting (BERBERIAN, 1981).

The graben like the Qezel-Owzan basin must have been formed in an extensional tectonic regime. The Miocene sediments widely covering the basin, as found in the geological map (HAGHIPOUR and AGHANABATI, 1985), may indicate that subsidence of the basin took place during the Miocene. Other evidence for extensional phase in this geological time is the intrusion of alkaline and calc-alkaline volcanics (BERBERIAN and KING, 1981). It is probable that originally, marginal normal faults forming a basin and range system in the previous extensional stress field converted to reverse faults in the present compressional stress field.

7. Conclusions

1) The epicentral distribution of the aftershocks is described by the linear trend in the N60°W direction. The focal depths range from surface to 30 km. The region in the vicinity of the focus of the mainshock is a 10–20 km wide gap in the aftershock activity. The most remarkable cluster of shocks was observed at the southeastern end of the aftershock area.

2) At the margin of the Qezel-Owzan basin are longitudinal faults judging from the topographic map and the Landsat image. Moreover, there is a possible strike-slip fault in parallel with these faults on the uplifted side of the northern marginal fault. The left lateral offset is more than 1–2 km. The aftershocks are in line with this newly proposed fault.

3) It is inferred that the V_P/V_S ratio is rather high, the average being 1.88 ± 0.60, for the large tripartite network. For some events the ratio is reduced to around 1.74 as usually found in Japan, for instance.

4) A relatively high decay rate of the aftershock frequency was observed during the period between one month and five months after the mainshock. The p value for the modified Omori formula is 1.5.

5) Composite focal mechanism indicates the variant focal mechanisms for the aftershocks.

Acknowledgments

The authors thank Messrs. Cho Oyama, Itaru Takashio and Koji Asai of Ministry of Education, Japan, Mr. Yuichi Iizuka of Ministry of Foreign Affairs, Ambassador Kunihiko Saito, Messrs. Masayuki Kurihara and Tsuneshi Yoshikawa from Embassy of Japan in Tehran, Prof. Motohiko Hakuno, Director of Earthquake Research Institute (ERI), University of Tokyo, Prof. Katsuyuki Abe, Ms. Tomoko Mura-

kami and Yukari Nakao of ERI, Messrs. Hassan Taherian and Masud Maleki from Embassy of Islamic Republic of Iran in Tokyo, staff members of Institute of Geophysics, Tehran University, and the authority of Tehran University for encouraging and supporting our collaborative research work. Thanks are extended to Prof. Toshio Matsutani of University of Tokyo, Prof. Koji Kamioka of Tokyo University for Foreign Studies, and Mr. Kazuya Yamauchi, a postgraduate student of Waseda University, who is visiting Tehran University, for advising the Japanese authors on the way of life in Iran. We are also grateful to Mr. Hitoshi Suzuki of the Institute of Developing Economies for serving as an interpreter and assisting our observation work, Prof. Kazuyuki Koike of Komazawa University for providing us with the Landsat imagery, Dr. Yasutaka Ikeda of University of Tokyo for making for us the mosaic of the imagery and giving information concerning geomorphology, Prof. Tokihiko Matsuda of ERI for valuable suggestions for interpretation of the Landsat image, Prof. Yukimasa Yamada of Tokyo Metropolitan University for informing us of the features of the Iranian architecture, Dr. Masakazu Takahashi of Applied Geology Corp. Ltd., Dr. Kazuki Kudo of ERI for providing us printed matter from Iran, and Mr. Izumi Ogino of ERI for reproducing cassette tape data. This study was supported by a Grant-in-Aid for Monbusho International Scientific Research Program (Joint Research) No. 02044171, Ministry of Education, Science and Culture, Japan.

References

AKASHEH, B., 1975, Travel time residuals in the Iranian plateau, *J. Geophys.*, **41**, 281–288.

AMBRASEYS, N. N., 1963, The Buyin-Zara (Iran) earthquake of September, 1962 — A field report, *Bull. Seism. Soc. Am.*, **53**, 705–740.

ASTANEH, A. and M. G. ASHTIANY, 1990, The Manjil, Iran earthquake of June 21, 1990, *EERI SPECIAL EARTHQUAKE REPORT*, 5–13.

BERBERIAN, M. (ed.), 1976, Seismotectonic map of Iran, Geological Survey of Iran, Ministry of Mines and Metals.

BERBERIAN, M., 1981, Active faulting and tectonics of Iran, in *Zagros, Hindu Kush, Himalaya Geodynamic Evolution*, eds. Guputa, H. K. and F. M. Delany, *Geodyn. Ser., Am. Geophys. Un.*, **3**, 33–69.

BERBERIAN, M., 1982, Aftershock tectonics of the 1978 Tabas-e-Golshan (Iran) earthquake sequence: a documented active 'thin- and thick-skinned tectonic' case, *Geophys. J. Roy. Astr. Soc.*, **68**, 499–530.

BERBERIAN, M. and G. C. P. KING, 1981, Towards a paleogeography and tectonic evolution of Iran, *Can. J. Earth Sci.*, **18**, 210–265.

HAGHIPOUR, A. and A. AGHANABATI (eds.), 1985, Geological Map of Iran, Geological Survey of Iran, Ministry of Mines and Metals.

HIRATA, N. and M. MATSU'URA, 1987, Maximum-likelihood estimation of hypocenter with origin time eliminated using nonlinear inversion technique, *Phys. Earth Planet. Interiors*, **47**, 50–61.

IKAMI, A., S. ASANO, K. KOKETSU, T. MORIYA, K. ITO, T. TANADA, K. YOSHIDA, T. YABUKI and N. HIRATA, 1988, Crustal structure deduced from explosion observations, *Earth Monthly*, **10**, 687–693 (in Japanese).

JACKSON, J. and D. MCKENZIE, 1984, Active tectonics of the Alpine-Himalayan Belt between western Turkey and Pakistan, *Geophys. J. Roy. Astr. Soc.*, **77**, 185–264.

KENNETH, B. C., L. E. HEUCKROTH and R. A. KARIM, 1969, An investigation of the Dasht-e Bayaz, Iran, earthquake of August 31, 1968, *Bull. Seism. Soc. Am.*, **59**, 1793–1822.

KIKUCHI, M., K. SATAKE and H. KANAMORI, 1990, Source process of the Iran earthquake of June 20, 1990, *PROGRAMME* and *ABSTRACTS*, *Seism. Soc. Jpn.*, 1990, No. 2, 67 (in Japanese).

LE PICHON, X., 1968, Sea floor spreading and continental drift, *J. Geophys. Res.*, **73**, 3661–3697.

MATSU'URA, M., 1984, Baysian estimation of hypocenter with origin time eliminated, *J. Phys. Earth*, **32**, 469–483.

MCKENZIE, D., 1972, Active tectonics of the Mediterranean region, *Geophys. J. Roy. Astr. Soc.*, **30**, 109–185.

MOINFAR, A. A. and A. NADERZADEH, 1990, An immediate and preliminary report on the Manjil, Iran, earthquake of 20 June 1990, Building and Housing Research Center, Ministry of Housing and Urban Development, Islamic Republic of Iran, 68 pp. (in Persian with English abstract).

MORGAN, W. J., 1968, Rises, trenches, great faults and crustal blocks, *J. Geophys. Res.*, **73**, 1959–1982.

NEPROCHNOV, YU. P., 1968, Structure of the earth's crust of epi-continental seas: Caspian, Black, and Mediterranean, *Can. J. Earth Sci.*, **5**, 1037–1043.

NOWROOZI, A. A., 1972, Focal mechanism of earthquakes in Persia, Turkey, West Pakistan, and Afghanistan and plate tectonics of the Middle East, *Bull. Seism. Soc. Am.*, **62**, 823–850.

SHIKALIBEILY, E. Sh. and B. V. GRIGORIANTS, 1980, Principal features of the crustal structure of the south-Caspian basin and the conditions of its formation, *Tectonophysics*, **69**, 113–121.

TSUKUDA, T., K. NAKAMURA and Y. KISHIMOTO, 1977, The earthquake on Septembr 21, 1973 in the vicinity of the Yamasaki fault and its aftershock activity, *Zisin* 2, **30**, 151–162 (in Japanese with English abstract).

TSUKUDA, T., K. SAKAI, S. HASHIMOTO, M. R. GHEITANCHI, H. SUZUKI, S. SOLTANIAN and P. MOZAFFARI, 1991, A field study on various phenomena associated with the 1990 Rudbar, northwest Iran, earthquake, *Bull. Earthq. Res. Inst., Univ. Tokyo*, **66**, 419–454 (in Japanese with English abstract).

TSUKUDA, T., K. SATAKE, Y. HONKURA, S. B. UÇER and A. M. IŞIKARA, 1988, Low seismicity, low coda-Q and discontinuities of the upper crust in the vicinity of the Iznik-Mekece Fault, the North Anatolian Fault Zone, Turkey, *Bull. Earthq. Res. Inst., Univ. Tokyo*, **63**, 327–348.

TSUMURA, K., 1967, Determination of earthquake magnitude from total duration of oscillation, *Bull. Earthq. Res. Inst., Univ. Tokyo*, **45**, 7–18.

UNIVERSITY OF TOKYO, 1988, Seismic activities in the Kanto-Koshinetsu district (May–October, 1987), *Rep. Coord. Com. Earthq. Predict.*, **39**, 113–140 (in Japanese).

UTSU, T., 1969, Aftershocks and earthquake statistics (1) —Some parameters which characterize an aftershock sequence and their interrelations—, *J. Fac. Sci., Hokkaido Univ. Ser. VII*, **3**, 129–195.

YOSHIDA, Y., 1990, Focal mechanism solution of the Iran earthquake of June 20, 1990, *POSEIDON TSUSHIN* (News letter for the POSEIDON (Pacific Orient Seismic Digital Observation Network) project), No. 17 (in Japanese).

1990 年イラン北西部ルードバール地震 (M 7.3) の余震分布とそのテクトニクス的意味

東京大学地震研究所
佃　為成
酒井　要
橋本信一
M. R. GHEITANCHI

テヘラン大学地球物理研究所
S. SOLTANIAN
P. MOZAFFARI
N. MOZAFFARI
B. AKASHEH
A. JAVAHERIAN

1990 年 6 月 20 日 21 時 00 分 13.12 秒（世界時），イラン北西部ギーラーン州のルードバール市付近で M 7.3 の浅発地震が発生した．地震の 30 日後から余震観測を実施した．60 km のスパンの 3 点観測網 (Saravan, Abbar, Abtorsh) による観測は 5 ケ月以上の期間続けられた．ほかに 3 ケ所において 2～5 日間の短期観測 (Masuleh, Bivarzin, Jirandeh) をおこなった．

長期 3 点観測網には 790 個の地震が少なくとも 1 点で記録された．マグニチュード分布を見ると M 3 以上で均一に記録されたと判断できる．このうち 3 点で記録されたのは 67 個，S-P 時間が少なくとも 1 点以上で読めたものが 54 個，震源が決定できたものは 39 個である．また，短期観測点のデータを含め，4 ないし 6 点で震源決定できたものは 20 個であった．

余震は西北西-東南東走向の細長い分布を示す．長さは，90 km, 幅は 20 km である．深さは精度に問題があるが，だいたい 20～30 km より浅い．本震の震源より南東側の部分に余震が多い．その南東端に集中する地震群の深さは近くの観測点の S-P 時間分布から 16 km より浅いことが分かった．余震分布の走向は Qezel-Owzan 川が流れる盆地を画する一対の縦ずれの活断層のそれと一致し，その隆起側に今回の地震が発生した．Landsat の衛星写真と地形図の判読から余震域に沿った左横ずれの活断層の存在が予想される．尾根の屈曲から推定されるずれの量は 1～2 km 以上である．

余震の発震機構をしらべるため，初動の押し引きの重ね合わせを試みたが，系統的な断層面解を得ることはできなかった．

本震後 30 日から 180 日間の余震回数は改良大森公式 (p=1.5) に従って時間とともに減少した．しかし，観測開始の頃（7 月 22～26 日）は余震の減衰が甚だしく，p=4.0 ぐらいの値を示す．